# Technical Note: **A novel parameterization of the transmissivity due to ozone absorption in the *k*-distribution method and correlated-*k* approximation of Kato et al. (1999) over the UV band**

**W. Wandji Nyamsi[1], A. Arola[2], P. Blanc[1], A. V. Lindfors[2], V. Cesnulyte[2,3], M. R. A. Pitkänen[2,3], and L. Wald[1]**

[1]{ MINES ParisTech, PSL Research University, O.I.E. - Centre Observation, Impacts, Energy - Sophia Antipolis, France }

[2]{ Finnish Meteorological Institute, Kuopio, Finland }

[3]{ Department of Applied Physics, University of Eastern Finland, Kuopio, Finland }

Correspondence to: W. Wandji Nyamsi (william.wandji@mines-paristech.fr)

## Abstract

The *k*-distribution method and the correlated-*k* approximation of Kato et al. (1999) is a computationally efficient approach originally designed for calculations of the broadband solar radiation at ground level by dividing the solar spectrum in 32 specific spectral bands from 240 nm to 4606 nm. Compared to a spectrally-resolved computation, its performance in the UV band appears to be inaccurate, especially in the spectral intervals #3 [283, 307] nm and #4 [307, 328] nm because of inaccuracy in modelling the transmissivity due to ozone absorption. Numerical simulations presented in this paper indicate that a single effective ozone cross section is insufficient to accurately represent the transmissivity over each spectral interval. A novel parameterization of the transmissivity using more quadrature points yields maximum error of respectively 0.0006 and 0.0143 for interval #3 and #4. How to practically implement this new parameterization in a radiative transfer model is discussed for the case of libRadtran. The new parameterization considerably improves the accuracy of the retrieval of irradiances in UV bands.

## 1. Introduction

Radiative Transfer Models (RTM) are often used to provide estimates of the UV irradiance.

One of the difficulties in the computation lies in taking into account the gaseous absorption cross sections that are highly wavelength dependent (Molina and Molina, 1986). For instance, the ozone cross section changes by more than two orders of magnitude over the UV band [280, 400] nm. The best estimate of the UV irradiance is made by a spectrally-resolved calculation of the radiative transfer for each wavelength followed by integration over the UV band. However, such spectrally detailed calculations are computationally expensive. Therefore, several methods have been proposed to reduce the number of calculations. Among them, are the *k*-distribution method and the correlated-*k* approximation proposed by Kato et al. (1999). It is originally designed for providing a good estimate of the total surface solar irradiance by using 32 specific spectral intervals across the solar spectrum from 240 nm to 4606 nm. Hereafter, these spectral intervals are abbreviated in KB (Kato bands). The Kato et al. method is implemented in several RTMs and is a very efficient way to speed up computations of the total surface solar irradiance. Its performance over the UV band is not very accurate when compared to detailed spectral calculations made with libRadtran (Mayer et al., 2005) or SMARTS (Gueymard, 1995).

For a spectral interval $\Delta\lambda$ where λ is the wavelength, let $I_{0\Delta\lambda}$ and $I_{\Delta\lambda}$ denote respectively the irradiance on a horizontal plane at the top of atmosphere and at surface, the spectral clearness index $KT_{\Delta\lambda}$, also known as spectral global transmissivity of the atmosphere, or spectral atmospheric transmittance, or spectral atmospheric transmission, is defined as:

$$KT_{\Delta\lambda} = \frac{I_{\Delta\lambda}}{I_{0\Delta\lambda}} \quad (1)$$

Wandji Nyamsi et al. (2014) compared $KT_{\Delta\lambda}$ obtained by the correlated-*k* approach against that obtained by spectrally resolved computations using libRadtran and SMARTS, both for clear-sky and cloudy conditions for a set of realistic atmospheric and cloud coverage states, and for each KB. They found that the Kato et al. method underestimates transmissivity in KB #3 [283, 307] nm and #4 [307, 328] nm covering the UV range by respectively -93% and -16% in relative value and exhibits relative root mean square error of 123% and 17% in clear-sky conditions. Similar relative errors are observed for cloudy conditions.

The underestimation for these two bands can be explained by the fact that Kato et al. (1999) assume that the ozone cross section at the center wavelength in each interval represents the absorption over the whole interval. The ozone cross sections were taken from WMO (1985). Actually, the ozone cross section is strongly dependent on the wavelength in the UV region

(Molina and Molina, 1986). Both KB #3 and #4 in the UV range are large for considering only a single value of ozone cross section.

In order to improve the potential of Kato et al. method for estimating narrow band UV irradiances, in particular for the KBs #3 and #4, a new parameterization is proposed for the transmissivity due to the sole ozone absorption. Then, for each spectral interval, an assessment of the performance of the new parameterization in representing this transmissivity is made for a wide range of realistic cases against detailed spectral calculations. A short section describes how to implement this parameterization in the practical case of the RTM libRadtran 1.7. Finally, in each KB, the performance of the new parameterization is assessed when the direct normal, upward, downward and global irradiances at different altitudes are computed.

## 2. Transmissivity due to ozone absorption

The average transmissivity $T_{o3\Delta\lambda}$ due to the sole ozone absorption for *Δλ* can be defined by Eq. (2).

$$T_{o3\Delta\lambda} = \frac{\int_{\Delta\lambda} I_{0\lambda} e^{-k_\lambda \frac{u}{\mu_0}} d\lambda}{\int_{\Delta\lambda} I_{0\lambda}\, d\lambda} \quad (2)$$

where $I_{o\lambda}$ is the spectral irradiance at the top of the atmosphere on a horizontal plane, $k_\lambda$ the ozone cross section at $\lambda$, $u$ the amount of ozone in the atmospheric column and $\mu_0$ the cosine of the solar zenith angle.

A technique widely used for computing $T_{o3\Delta\lambda}$ is based on a discrete sum of selected exponential functions (Wiscombe and Evans, 1977):

$$T^n_{o3\Delta\lambda} \ = \sum_{i=1}^{n} a_i\, e^{-k_i\, u/\mu_0}. \quad (3)$$

where $\{k_i\}$ are the effective ozone cross sections and $\{a_i\}$ are the weighting coefficients obeying $\sum_{i=1}^{n} a_i = 1$.

In the Kato et al. method, only one exponential function (*n=1*) is used for each KB to estimate the average transmissivity $T_{o3_{KB}}$:

$$T_{o3_{KB}} = e^{-k_{KB}\frac{u}{\mu_0}}. \quad (4)$$

Kato et al. (1999) have chosen the ozone cross section at the central wavelength for each KB #3 or KB #4 for a temperature of 203 K: $k_{KB3} = 5.84965\ 10^{-19}$ cm$^2$ and $k_{KB4} = 4.32825\ 10^{-20}$ cm$^2$.

## 3. Effective ozone cross section

Is there a single effective ozone cross section that may represent the absorption over the whole interval? In that case, this effective cross section $k_{eff}$ is determined for each KB from the combination of Eqs (2) and (3) with $n$ = 1:

$$T_{o3_{eff}} = e^{-k_{eff}\frac{u}{\mu_0}} = \frac{1}{I_{0\Delta\lambda}} \int_{\Delta\lambda} I_{0\lambda} e^{-k_\lambda \frac{u}{\mu_0}} d\lambda. \quad (5)$$

This equation may be rewritten

$$k_{eff}\ \frac{u}{\mu_0} = -\ln \frac{1}{I_{0\Delta\lambda}} \int_{\Delta\lambda} I_{0\lambda} e^{-k_\lambda \frac{u}{\mu_0}} d\lambda. \quad (6)$$

Several simulations are made to study this hypothesis. The ozone cross sections are those from Molina and Molina (1986) at 226 K, 263 K and 298 K, and the top-of-atmosphere solar spectrum of Gueymard (2004) is used. The ozone cross sections at 203 K are obtained by linear extrapolation for each wavelength (Fig. 1). Samples of 10000 pairs $(\mu_0, u)$ were generated by a Monte-Carlo technique. The random selection of the solar zenith angles follows a uniform distribution in [0°, 80°]. Similarly to what was done by Lefevre et al. (2013) and Oumbe et al. (2014), $u$ is computed in Dobson unit as:

$$u = 300\beta + 100 \quad (7)$$

where $\beta$ follows the beta distribution with A parameter = 2, and B parameter = 2.

The 10000 simulations yield a set **X** of ( $\frac{u}{\mu_0}$ ) and a set **Y** of values $-\ln \frac{1}{I_{0\Delta\lambda}} \int_{\Delta\lambda} I_{0\lambda} e^{-k_\lambda \frac{u}{\mu_0}} d\lambda$ . Eq. (6) is then

$$k_{eff}\ \mathrm{X} = \mathrm{Y} \quad (8)$$

and $k_{eff}$ can be found by least-square fitting technique. For the KB #3 and #4, the values obtained are respectively $k_{eff3}$ $=2.29\ 10^{-19}$ cm$^2$ and $k_{eff4}=2.65\ 10^{-20}$ cm$^2$. The average transmissivity $T_{o3_{eff}}$with the effective ozone cross section is then computed by Eq. (5).

Estimated transmissivities $T_{o3_{KB}}$ and $T_{o3_{eff}}$ computed with Eq. (4) and Eq. (5) using a second set of 10000 pairs $(\mu_0, u)$ randomly selected are compared to the reference transmissivity $T_{o3\Delta\lambda}$ computed with Eq. (2) for each KB (Fig. 2). In KB #3, $T_{o3_{KB}}$ (red line) strongly underestimates $T_{o3\Delta\lambda}$ meaning that the single ozone cross section adopted by Kato et al. is too large. On the contrary, $T_{o3_{eff}}$ (blue line) exhibits a large overestimation meaning that the efficient ozone cross section $k_{eff}$ is too low. That may be explained by the fact that the solar radiation at the short wavelengths is completely absorbed and therefore becomes somewhat unimportant for the effective ozone cross sections. In this interval, the ozone cross section is strongly variable as shown in Fig. 1. Since $k_{eff}$ is the optimal value reducing as much as possible the discrepancy between $T_{o3_{eff}}$ and $T_{o3\Delta\lambda}$, it may be concluded that a single effective ozone cross section may not accurately represent the absorption over the whole KB #3.

In KB #4, $T_{o3_{KB}}$ (red line) noticeably underestimates $T_{o3\Delta\lambda}$ meaning that the single ozone cross section adopted by Kato et al. is too large. $T_{o3_{eff}}$ is closer to $T_{o3\Delta\lambda}$ though it exhibits underestimation when $T_{o3\Delta\lambda} < 0.47$ and overestimation when $T_{o3\Delta\lambda} > 0.47$. Like previously stated, it may be concluded that a single effective ozone cross section may not accurately represent the absorption over the whole KB #4.

## 4. New parameterization

The new parameterization $T_{o3_{new}}$ for computing $T_{o3\Delta\lambda}$ consists in using Eq. (3) with *n* greater than 1 but as small as possible to decrease the number of calculations while retaining a sufficient accuracy. *n* can be seen as the number of sub-intervals $\delta\lambda_i$ included in $\Delta\lambda$ for which effective ozone cross section and weighting coefficients can be defined. The greater the *n*, the greater the number of calculations, the more accurate the modelling of $T_{o3\Delta\lambda}$.

Many solutions are possible. No systematic scan of possible solutions in *n*, weight $a_i$ and $\delta\lambda_i$ was made. This could be a further work that is computationally expensive and that requires setting up a protocol for selection of the best trade-off between accuracy and number of calculations. Here, a few tests were made with *n* ranging from 2 to 5. The best trade-off was found at *n*=4. A further study was performed for *n*=4 by adopting equal weights for the sub-intervals for both KB #3 and #4. It comes:

$$T_{o3_{new}} = \sum_{i=1}^{4} 0.25\, e^{-k_i\, u/\mu_0}, \qquad (9)$$

where $k_i$ is the effective ozone cross section for each of the four sub-intervals. This proposed solution is of empirical nature. Using a third set of 10000 randomly selected pairs$(\mu_0, u)$, from which $T_{o3\Delta\lambda}$ is computed (Eq. 2), the optimal sets of four $k_i$ and four sub-intervals $\delta\lambda_i$ minimizing the discrepancy between $T_{o3\Delta\lambda}$ and $T_{o3_{new}}$ is obtained by using the algorithm of Levenberg-Marquardt. Table 1 gives for each KB, the sub-intervals and their corresponding effective ozone cross section $k_i$, weight $a_i$ for computing $T_{o3_{new}}$. The advantage is that such parameterization is defined once for all.

To assess the performance of this new parameterization, reference transmissivity $T_{o3\Delta\lambda}$ and estimated transmissivity $T_{o3_{new}}$ are computed with respectively Eq. (2) and Eq. (9) using a fourth set of 10000 pairs $(\mu_0, u)$ randomly selected and are compared to each other for each KB (Fig. 3). In this validation step, the random selection of the solar zenith angles follows a uniform distribution in [0°, 89°]. Statistical indicators are given in Table 2 for each KB. In general, for both KBs, the squared correlation coefficient is greater than 0.99 with very low scattering. $T_{o3_{KB}}$ (red line) is also reported in Fig. 3. The difference between $T_{o3_{KB}}$ and $T_{o3_{new}}$ is striking. In each KB, $T_{o3_{new}}$ is almost equal to $T_{o3\Delta\lambda}$ in all cases. While the mean value for $T_{o3\Delta\lambda}$ is respectively 0.0287 for KB #3 and 0.5877 for KB #4 for this data set, the maximum error in absolute value in transmissivity is respectively 0.0006 and 0.0143.

## 5. Practical implementation in Radiative Transfer Model: the case of libRadtran 1.7

The file *o3.dat* in libRadtran 1.7 depicts ozone absorption. In the corresponding file, a header of seven lines describes the meanings of the following three columns. The first column contains the number of the spectral interval: KB #1 to 32. The second one gives the number of quadrature points in each KB; the value is 1 in UV bands. The third column can be either the value of the single ozone cross section in each wavelength interval expressed in cm$^2$ or -1 when the number of quadrature point is greater than one. In this last case, libRadtran refers to netcdf file *cross_section.table._O3.noKB.cdf* -where *noKB* is the number of the KB- that contains the weight, the effective ozone cross section dependent of temperature and pressure.

Including the new parameterization needs two actions. Firstly, for KB #3 and KB #4, set the second column to 4 and the third column to -1. Secondly, create two netcdf files named *cross_section.table._O3.03.cdf* and *cross_section.table._O3.04.cdf* containing for each interval their corresponding weight and effective cross sections given in Table 1.

## 6. Performance of the new parameterization in calculating irradiances in the KB #3 and #4 in clear-sky conditions

This section presents the errors made by using the new parameterization in calculating irradiances in the KB #3 and #4. To that extent, a set of 10000 atmospheric states have been randomly built following the marginal distribution variables described in Table 2 of Wandji Nyamsi et al. (2014), except solar zenith angle varying uniformly between 0° and 89°. Each atmospheric state is input to libRadtran which is run twice for the KB #3 and #4: one with detailed spectral calculations, and the second with the new parameterization. The RTM libRadtran provides irradiance components that are called “direct normal” that is the irradiance received from the direction of the Sun in a plane normal to the sun rays, “downward” that is the diffuse irradiance, “upward” that is the upwelling irradiance, and “global” that is the sum of the diffuse and direct irradiances, the latter being projected on a horizontal plane. Each run of libRadtran produces a set of these components at various altitudes above ground level, from 0 to 50 km, and the deviations between the irradiances produced by each run: new parameterization minus detailed spectral calculations, are computed.

The deviations are summarized by the bias, root mean square error (RMSE) and the correlation coefficient for each altitude and in each KB (Tables 3 and 4). The biases and RMSE at each altitude are summarized in Figure 4 for both KBs. The squared correlation coefficient is greater than 0.999 in most cases with a minimum at 0.992. This demonstrates that the new parameterization reproduces well the changes in irradiance in all cases.

The direct normal irradiance increases with altitude and exhibits negative and positive bias in both KB #3 and #4. The bias varies as a function of the altitude. In KB #3, it reaches a minimum of -0.009 W $m^{-2}$ (-5% of the mean irradiance) at altitude 5 km, then increases with altitude up to a maximum of 0.453 W $m^{-2}$ (8%) at 35 km and suddenly decreases. The RMSE follows a slightly different pattern, with a decrease from 0.011 W $m^{-2}$ (18% of the mean irradiance) at surface down to a minimum 0.007 W $m^{-2}$ (3%) of at altitude 10 km, then increases with altitude till a maximum of 0.476 W $m^{-2}$ (8%) at 35 km and suddenly decreases. The bias and RMSE in KB #4 are less dependent with altitude. The bias is slightly negative at ground level: -0.043 W $m^{-2}$ (-3%), then increases with altitude till a maximum of 0.097 W $m^{-2}$ (1%) at 20 km and gently decreases down to -0.105 W $m^{-2}$ (-1% of the mean irradiance). The RMSE is fairly constant and ranges between a minimum of 0.039 W $m^{-2}$ (1%, 5 km) and a maximum of 0.132 W $m^{-2}$ (1%, 25 km).

The downward irradiance decreases with altitude. The bias is positive in both KB #3 and #4. It is fairly constant with altitude in KB #3, fluctuating between 0 and 0.007 W $m^{-2}$ (9%). The bias in KB #4 decreases with altitude, from a maximum of 0.108 W $m^{-2}$ (5%, 5 km) down to 0.000 W $m^{-2}$ at altitude 50 km. In both KB, the RMSE tends to decrease with altitude, from a maximum of 0.011 W $m^{-2}$ (14%, 5 km), respectively 0.119 W $m^{-2}$ (6%, 5 km), down to 0 W $m^{-2}$ at altitude 50 km.

The upward irradiance is fairly constant with altitude in both KB #3 and #4. The bias and the RMSE are fairly constant with altitude in KB #3, fluctuating respectively between -0.002 W $m^{-2}$ (-2%, 0 km) and 0.006 W $m^{-2}$ (12%, 50 km), and between 0.004 W $m^{-2}$ (5%, 0 km) and 0.007 W $m^{-2}$ (9%, 15 km). The bias and RMSE in KB #4 increase with altitude. The minimum and maximum are respectively 0.035 W $m^{-2}$ (1%, 0 km) and 0.141 W $m^{-2}$ (6%, 50 km), and 0.006 W $m^{-2}$ (3%, 0 km) and 0.155 W $m^{-2}$ (6%, 50 km).

The global irradiance increases with altitude and exhibits negative and positive bias in both KB #3 and #4. The bias varies as a function of the altitude. In KB #3, similarly to the case of the direct normal irradiance, the bias exhibits a minimum of -0.004 W $m^{-2}$ (-3%) at surface, then increases with altitude up to 0.327 W $m^{-2}$ (8%) at 35 km and suddenly decreases down to 0.010 W $m^{-2}$ (0%) at 50 km. The RMSE follows a similar trend, with a minimum of 0.005 W $m^{-2}$ (2%) at altitude 5 km, then increases up to 0.373 W $m^{-2}$ (9%) at 35 km and suddenly decreases down to 0.034 W $m^{-2}$ (1%) at 50 km. The situation is different in KB #4 where the bias and RMSE are less dependent with altitude. The bias is small and fluctuates between a minimum of -0.070 W $m^{-2}$ (-1%) at 50 km and a maximum of 0.100 W $m^{-2}$ (2%, 10 km). The RMSE is fairly constant and ranges between a minimum of 0.042 W $m^{-2}$ (1%, 30 km) and a maximum of 0.111 W m$^{-2}$ (2%, 10 km).

A similar comparison was made by Wandji Nyamsi et al. (2014) with the original approach of Kato et al. (1999) but for altitudes varying between 0 and 3 km. They reported relative bias, relative RMSE and $R^2$ for the spectral clearness index $KT_{\Delta\lambda}$ of respectively -92%, 123% and 0.718 for KB #3 and -16%, 17% and 0.991 for KB #4. For the new parameterization, with altitudes in the range [0, 3] km, the same quantities are respectively -2%, 4% and 0.999 for KB #3, and -2%, 3% and 0.999 for KB #4. The new parameterization improves considerably the irradiances estimated in KB #3 and KB #4.

## 7. Conclusion

The present paper has shown the inadequacy of parameterization of the transmissivity due to the sole ozone absorption based on a single ozone cross section for the bands KB #3 [283, 307] nm and KB #4 [307, 328] nm in the *k*-distribution method and correlated-*k* approximation of Kato et al. (1999). A novel parameterization using more quadrature points better represents the transmissivity with maximum error of respectively 0.0006 and 0.0143 for interval KB #3 and #4. The estimates of the various components of the irradiance: direct normal, downward, upward, global, in these Kato bands by using the new parameterization are considerably improved when compared to detailed spectral calculations. The squared correlation is greater than 0.992 in any case, and greater than 0.999 in most cases. The bias and RMSE vary with the altitude but are never greater than 0.5 W m$^{-2}$ for the direct normal or global in KB #3, and 0.1 W m$^{-2}$ in KB #4. They are smaller in KB #3 for the downward and upward irradiances: 0.01 W m$^{-2}$, and similar in KB #4: 0.1 W m$^{-2}$.This novel parameterization opens the way for more accurate estimates of the irradiance at surface in the UV range, and possibly in narrower spectral bands such as UV-A and UV-B.

## Acknowledgements

The authors thank the teams developing libRadtran (http://www.libradtran.org) and SMARTS and the referees whose remarks help in improving the content of the article. This work was partly funded by the French Agency ADEME in charge of energy (grant no. 1105C0028, 2011-2016) and took place within the Task 46 “solar resource assessment and forecasting” of the Solar Heating and Cooling programme of the International Energy Agency. William

Wandji Nyamsi has benefited from a personal grant of Foundation MINES ParisTech for a three-months visit to the Finnish Meteorological Institute.

## References

Lefèvre, M., Oumbe, A., Blanc, P., Espinar, B., Gschwind, B., Qu, Z., Wald, L., M. Schroedter-Homscheidt, Hoyer-Klick, C., Arola, A., Benedetti, A., Kaiser, J.W., and Morcrette, J.-J.: McClear: a new model estimating downwelling solar radiation at ground level in clear-sky conditions, Atmos. Meas. Tech, 6, 2403-2418, 2013.

Gueymard, C.: SMARTS2, Simple model of the atmospheric radiative transfer of sunshine: algorithms and performance assessment, Report FSEC-PF-270-95, Florida Solar Center, Cocoa, FL., USA, 78 pp.,1995.

Gueymard, C.: The sun's total and the spectral irradiance for solar energy applications and solar radiations models, Sol. Energy, 76, 423-452, 2004.

Kato, S., Ackerman, T., Mather, J., and Clothiaux, E.: The *k*-distribution method and correlated-*k* approximation for shortwave radiative transfer model, J. Quant. Spectrosc. Radiat. Transf., 62, 109-121, 1999.

Mayer, B., and Kylling, A.: Technical note: The libRadtran software package for radiative transfer calculations-description and examples of use, Atmos. Chem. Phys, 5, 1855-1877, 2005.

Molina, L. T., and Molina, M. J.: Absolute absorption cross sections of ozone in the 185- to 350-nm wavelength range, J. Geophys. Res., 91, 14501-14508. 1986.

Oumbe, A., Qu, Z., Blanc, P., Lefèvre, M., Wald, L., and Cros, S.: Decoupling the effects of clear atmosphere and clouds to simplify calculations of the broadband solar irradiance at ground level, Geosci. Model Dev., 7, 1661-1669, 2014.

Wandji Nyamsi, W., Espinar, B., Blanc, P., and Wald, L.: How close to detailed spectral calculations is the *k*-distribution method and correlated-*k* approximation of Kato et al. (1999) in each spectral interval?, 23 (5), 547-556, 2014, doi: 0.1127/metz/2014/0607.

Wiscombe, W. J., and Evans, J. W.: Exponential-Sum fitting of radiative transmission functions, J. Comput. Phy., 24 (4), 416–444, 1977.

WMO: Atmospheric ozone 1985, World Meteorological Organization Global ozone research and monitoring project, Report no. 16, Geneva, Switzerland, 520 p., 1985.

Table 1: Sub-intervals, effective ozone absorption coefficient and weight in each wavelength interval for computing $T_{o3_{new}}$.

| Interval Δλ, nm | Sub-interval $\delta\lambda_i$, nm | Effective ozone cross section $k_i$ ($10^{-19} cm^2$) | Weight $a_i$ |
|---|---|---|---|
| KB #3 283-307 | 283-292 | 11.360 | 0.250 |
| | 292-294 | 8.551 | 0.250 |
| | 294-301 | 3.877 | 0.250 |
| | 301-307 | 1.775 | 0.250 |
| KB #4 307-328 | 307-311 | 0.938 | 0.250 |
| | 311-321 | 0.350 | 0.250 |
| | 321-323 | 0.153 | 0.250 |
| | 323-328 | 0.076 | 0.250 |

Table 2: Statistical indicators by using the new parameterization for computing the transmissivity due to the sole ozone absorption in each Kato band. N° is the number of KB, $R^2$ is the squared correlation coefficient, Mean is the mean value of the reference average transmissivity, $\varepsilon$ is the maximum error.

| N° | Mean | Bias | RMSE | rBias (%) | rRMSE (%) | $R^2$ | $\varepsilon$ |
|---|---|---|---|---|---|---|---|
| KB # 3 | 0.0287 | -0.0004 | 0.0004 | -1.32 | 1.49 | 0.999 | 0.0006 |
| KB # 4 | 0.5877 | -0.0005 | 0.0030 | -0.08 | 0.52 | 0.999 | 0.0143 |

Table 3. Statistical indicators of the performances of the new parameterization for computing the irradiances in Kato band # 3 at different altitudes above ground level. “Mean” is the mean irradiance obtained from the detailed spectral calculations considered as reference.

| KB #3 | | | | | | | | |
|---|---|---|---|---|---|---|---|---|
| Altitude | Direct normal irradiance (W m$^{-2}$) | | | | Downward irradiance (W m$^{-2}$) | | | |
| (km) | Mean | Bias | RMSE | $R^2$ | Mean | Bias | RMSE | $R^2$ |
| 0 | 0.059 | -0.008 | 0.011 | 0.999 | 0.108 | 0.002 | 0.007 | 0.999 |
| 5 | 0.170 | -0.009 | 0.013 | 0.999 | 0.077 | 0.007 | 0.011 | 0.999 |
| 10 | 0.280 | -0.004 | 0.007 | 0.999 | 0.049 | 0.006 | 0.008 | 0.999 |
| 15 | 0.454 | 0.005 | 0.010 | 0.999 | 0.034 | 0.004 | 0.006 | 0.999 |
| 20 | 0.859 | 0.025 | 0.034 | 0.999 | 0.034 | 0.004 | 0.005 | 0.999 |
| 25 | 1.784 | 0.094 | 0.121 | 0.999 | 0.041 | 0.005 | 0.007 | 0.999 |
| 30 | 3.406 | 0.262 | 0.301 | 0.999 | 0.039 | 0.005 | 0.007 | 0.999 |
| 35 | 5.832 | 0.453 | 0.476 | 0.999 | 0.015 | 0.002 | 0.002 | 0.996 |
| 40 | 8.436 | 0.408 | 0.433 | 0.998 | 0.012 | 0.001 | 0.001 | 0.992 |
| 50 | 11.024 | 0.072 | 0.178 | 0.998 | 0.005 | 0.000 | 0.000 | 0.999 |
| Altitude | Upward irradiance (W m$^{-2}$) | | | | Global irradiance (W m$^{-2}$) | | | |
| (km) | Mean | Bias | RMSE | $R^2$ | Mean | Bias | RMSE | $R^2$ |
| 0 | 0.086 | -0.002 | 0.004 | 0.999 | 0.162 | -0.004 | 0.008 | 0.999 |
| 5 | 0.097 | 0.002 | 0.005 | 0.999 | 0.228 | 0.000 | 0.005 | 0.999 |
| 10 | 0.095 | 0.004 | 0.007 | 0.999 | 0.293 | 0.003 | 0.007 | 0.999 |
| 15 | 0.079 | 0.004 | 0.007 | 0.999 | 0.423 | 0.009 | 0.014 | 0.999 |
| 20 | 0.057 | 0.003 | 0.005 | 0.999 | 0.753 | 0.025 | 0.035 | 0.999 |
| 25 | 0.042 | 0.003 | 0.004 | 0.999 | 1.484 | 0.083 | 0.113 | 0.999 |
| 30 | 0.040 | 0.004 | 0.005 | 0.999 | 2.692 | 0.212 | 0.263 | 0.999 |
| 35 | 0.043 | 0.005 | 0.005 | 0.999 | 4.354 | 0.327 | 0.373 | 0.999 |
| 40 | 0.044 | 0.005 | 0.006 | 0.999 | 5.980 | 0.246 | 0.271 | 0.999 |
| 50 | 0.049 | 0.006 | 0.006 | 0.999 | 7.287 | 0.010 | 0.034 | 0.999 |

Table 4. Statistical indicators of the performances of the new parameterization for computing the irradiances in Kato band # 4 at different altitudes above ground level. “Mean” is the mean irradiance obtained from the detailed spectral calculations considered as reference.

| KB #4 | | | | | | | | |
|---|---|---|---|---|---|---|---|---|
| Altitude | Direct normal irradiance (W $m^{-2}$) | | | | Downward irradiance (W $m^{-2}$) | | | |
| (km) | Mean | Bias | RMSE | $R^2$ | Mean | Bias | RMSE | $R^2$ |
| 0 | 1.694 | -0.043 | 0.050 | 0.999 | 3.105 | 0.088 | 0.111 | 0.999 |
| 5 | 4.395 | -0.029 | 0.039 | 0.999 | 2.180 | 0.108 | 0.119 | 0.999 |
| 10 | 6.373 | 0.028 | 0.048 | 0.999 | 1.346 | 0.078 | 0.084 | 0.999 |
| 15 | 8.066 | 0.077 | 0.095 | 0.999 | 0.775 | 0.047 | 0.049 | 0.999 |
| 20 | 9.711 | 0.097 | 0.125 | 0.999 | 0.473 | 0.025 | 0.027 | 0.999 |
| 25 | 11.491 | 0.084 | 0.132 | 0.999 | 0.301 | 0.012 | 0.014 | 0.999 |
| 30 | 13.119 | 0.049 | 0.127 | 0.999 | 0.166 | 0.005 | 0.006 | 0.999 |
| 35 | 14.451 | -0.002 | 0.117 | 0.999 | 0.042 | 0.002 | 0.002 | 0.999 |
| 40 | 15.121 | -0.058 | 0.097 | 0.999 | 0.022 | 0.001 | 0.001 | 0.999 |
| 50 | 15.527 | -0.105 | 0.106 | 0.999 | 0.007 | 0.000 | 0.000 | 0.999 |
| Altitude | Upward irradiance (W $m^{-2}$) | | | | Global irradiance (W $m^{-2}$) | | | |
| (km) | Mean | Bias | RMSE | $R^2$ | Mean | Bias | RMSE | $R^2$ |
| 0 | 2.448 | 0.035 | 0.060 | 0.999 | 4.547 | 0.055 | 0.079 | 0.999 |
| 5 | 2.921 | 0.074 | 0.090 | 0.999 | 5.722 | 0.091 | 0.105 | 0.999 |
| 10 | 3.136 | 0.094 | 0.107 | 0.999 | 6.290 | 0.100 | 0.111 | 0.999 |
| 15 | 3.121 | 0.106 | 0.118 | 0.999 | 6.838 | 0.094 | 0.105 | 0.999 |
| 20 | 2.955 | 0.115 | 0.126 | 0.999 | 7.565 | 0.076 | 0.089 | 0.999 |
| 25 | 2.763 | 0.124 | 0.135 | 0.999 | 8.434 | 0.045 | 0.064 | 0.999 |
| 30 | 2.644 | 0.130 | 0.142 | 0.999 | 9.163 | 0.010 | 0.042 | 0.999 |
| 35 | 2.585 | 0.135 | 0.148 | 0.999 | 9.653 | -0.025 | 0.044 | 0.999 |
| 40 | 2.554 | 0.139 | 0.152 | 0.999 | 9.906 | -0.052 | 0.062 | 0.999 |
| 50 | 2.543 | 0.141 | 0.155 | 0.999 | 10.037 | -0.070 | 0.078 | 0.999 |

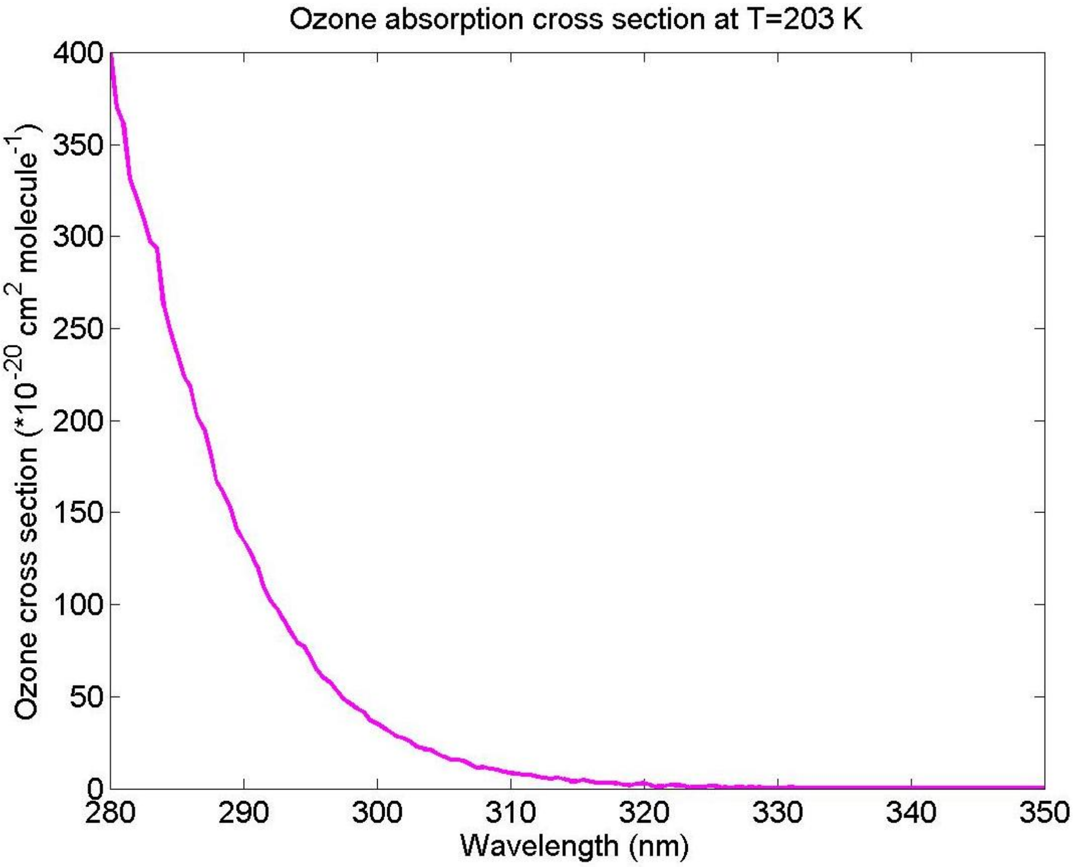


Figure 1. Ozone cross sections at 203 K as a function of the wavelength.

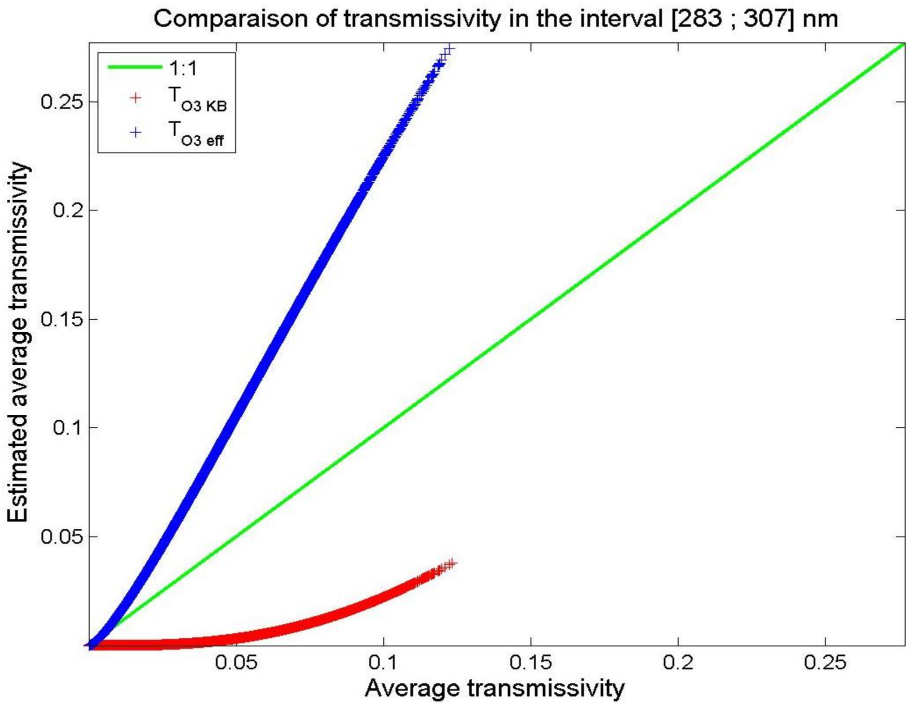


(a)

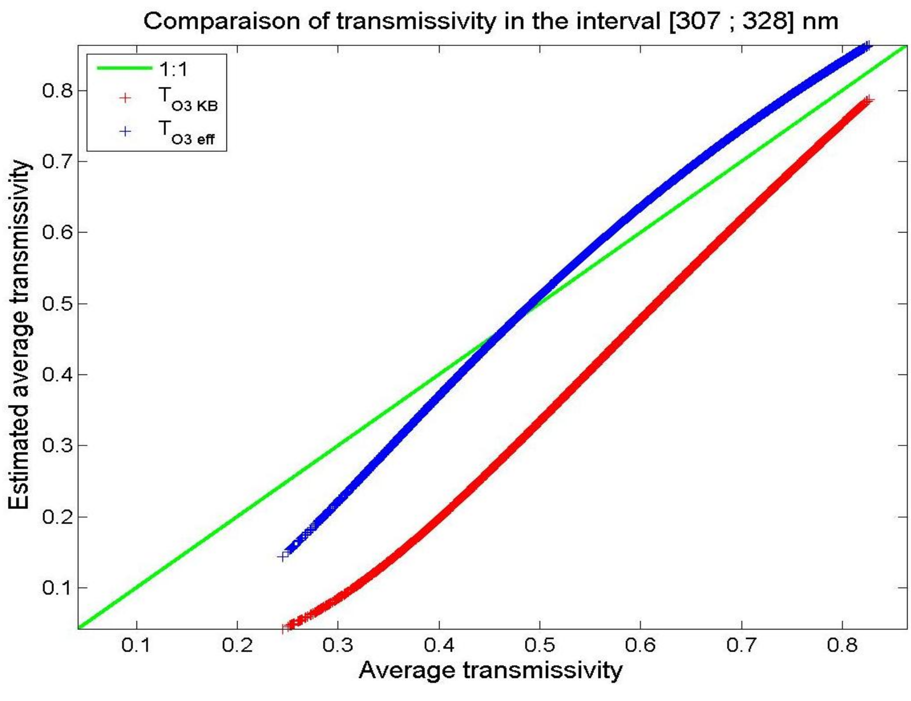


(b)

Figure 2. Scatterplot between average transmissivity $T_{o3\Delta\lambda}$ and the estimated $T_{o3_{KB}}$(red line) and $T_{o3_{eff}}$ (blue line) for (a) KB #3 [283, 307] nm; (b) KB #4 [307, 328] nm. The identity line is in green.

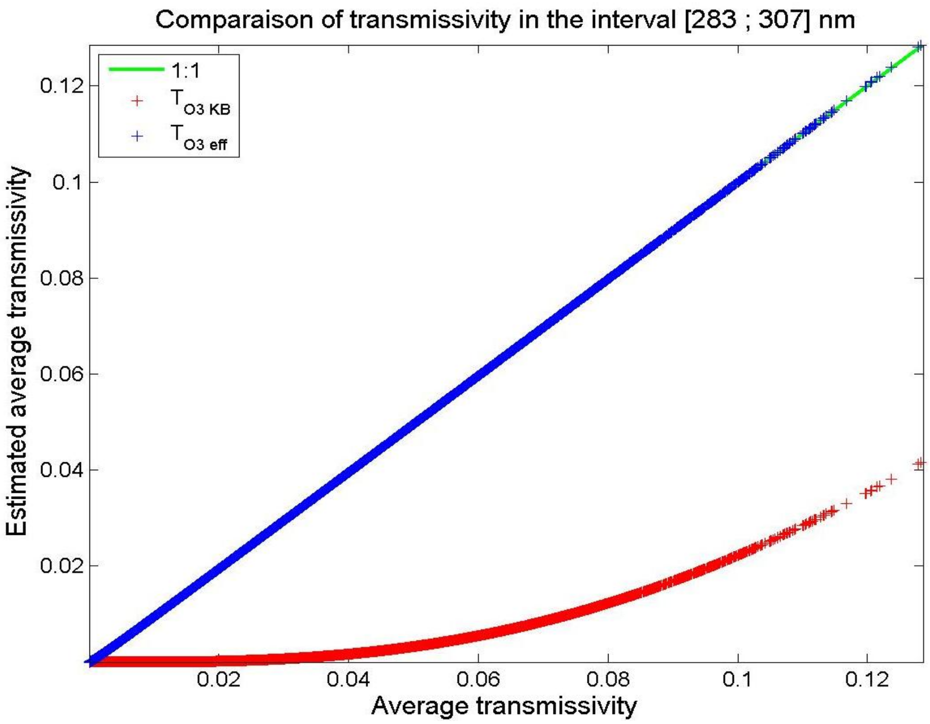


(a)

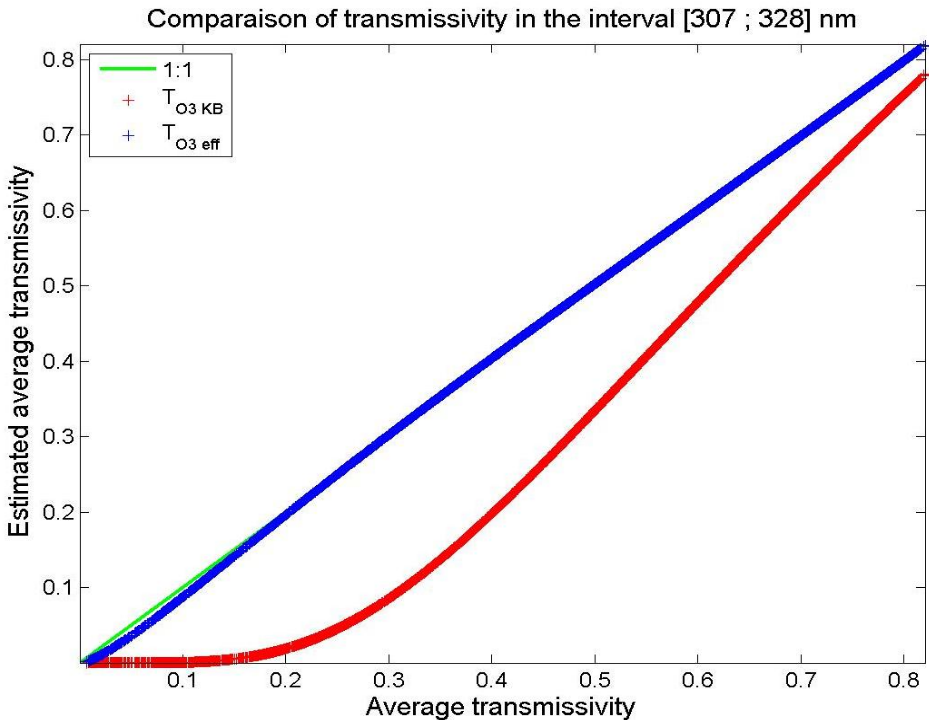


(b)

Figure 3. Scatterplot between average transmissivity $T_{o3\Delta\lambda}$ and the estimated $T_{o3_{KB}}$ (red line) and $T_{o3_{new}}$ (blue line) for (a) KB #3 [283, 307] nm; (b) KB #4 [307, 328] nm. The identity line is in green.

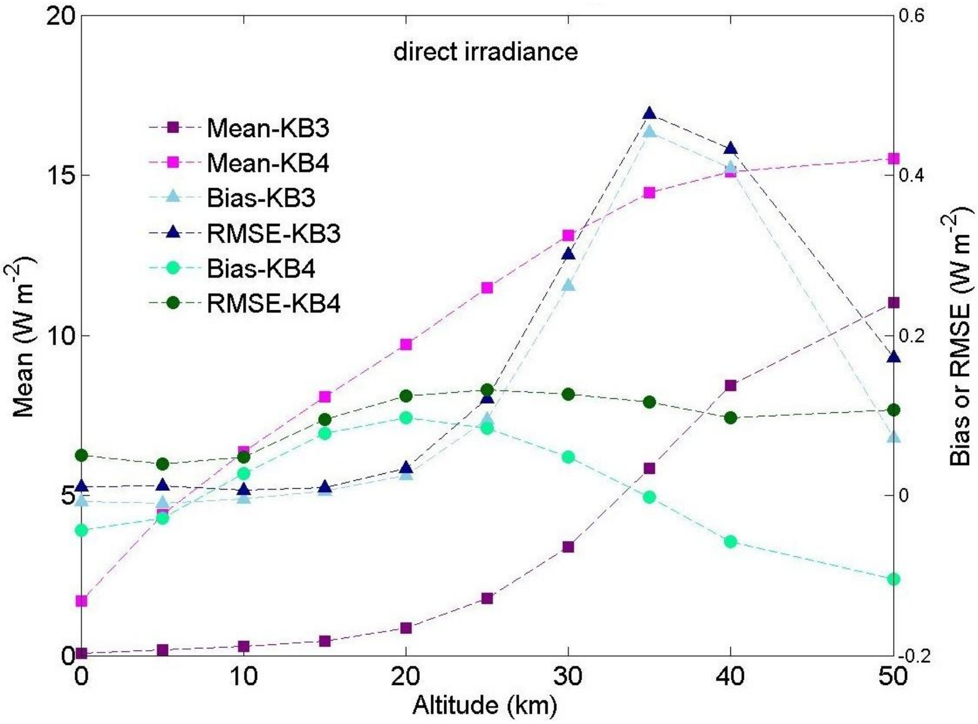
direct irradiance
Mean-KB3
Mean-KB4
Bias-KB3
RMSE-KB3
Bias-KB4
RMSE-KB4
Mean (W m-2)
Bias or RMSE (W m-2)
Altitude (km)

a)

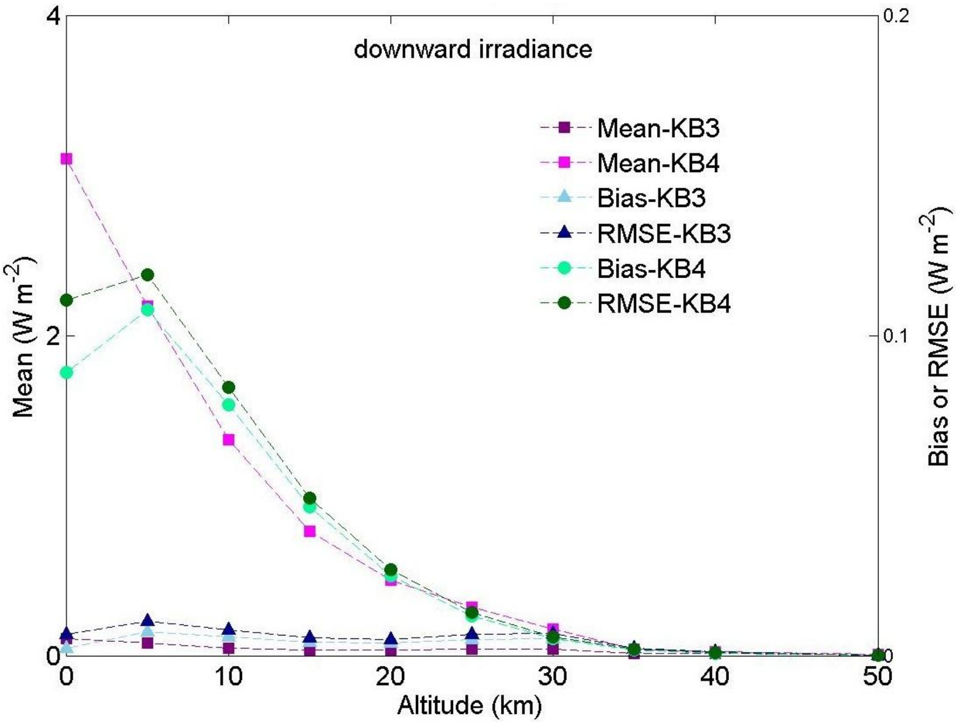
downward irradiance
Mean-KB3
Mean-KB4
Bias-KB3
RMSE-KB3
Bias-KB4
RMSE-KB4
Mean (W m-2)
Bias or RMSE (W m-2)
Altitude (km)

b)

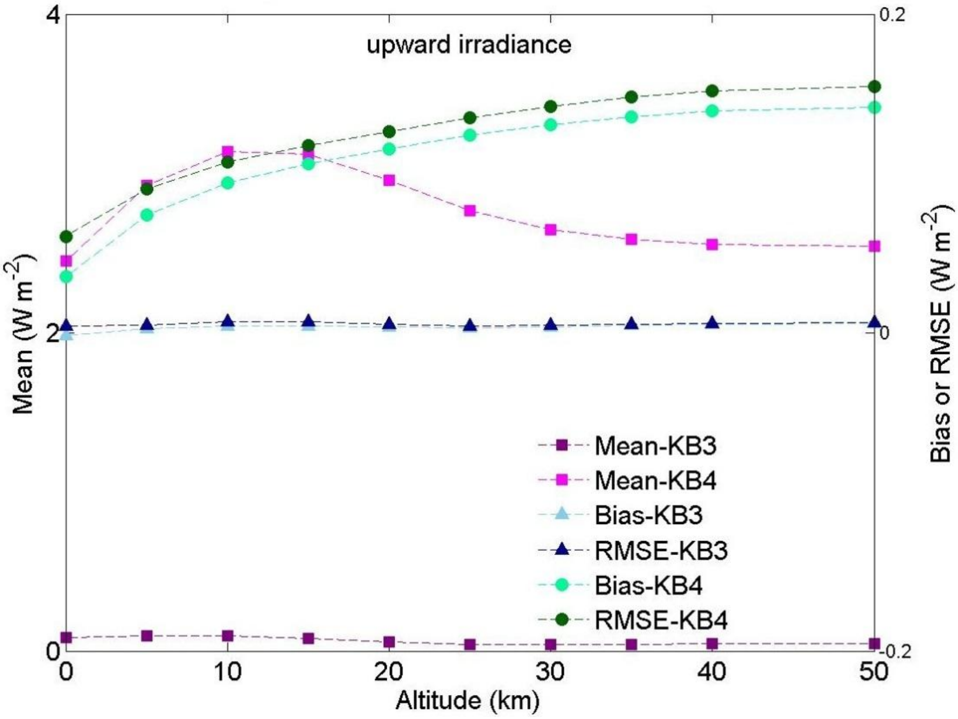


c)

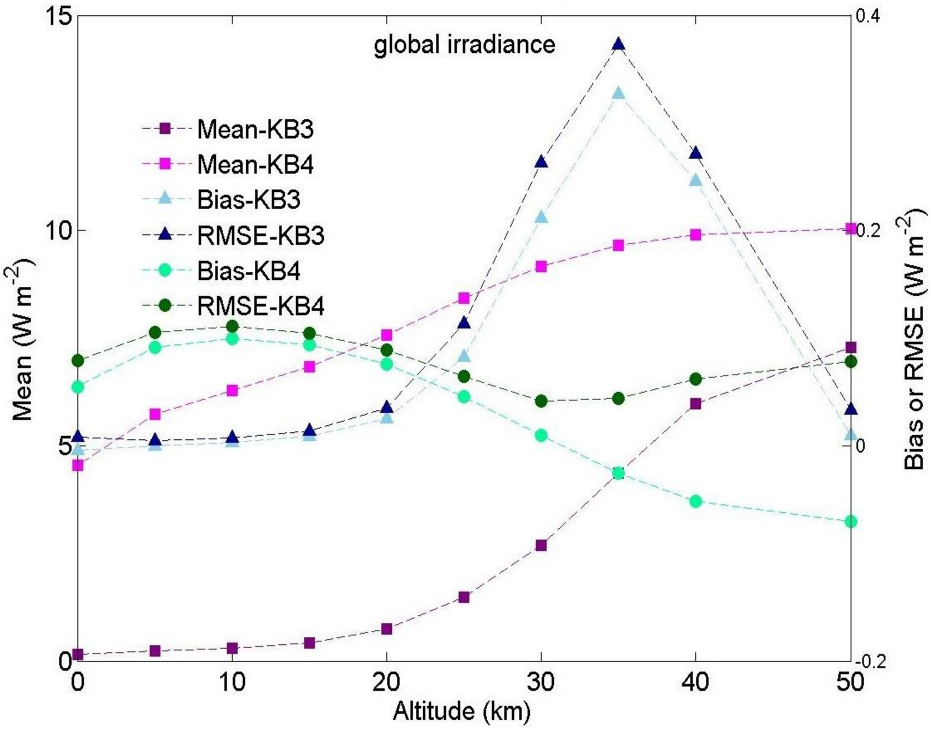


d)

Figure 4. Mean irradiances (left vertical axis), biases and RMSE (right vertical axis) at different altitudes in KB #3 and KB #4 for (a) direct normal, (b) downward, (c) upward and (d) global irradiance.